

FRONT MATTER

Title

• Immobilized ^{13}C -Labeled Polyether Chain Ends Confined to the Crystallite Surface Detected by Advanced NMR

• ^{13}COO Chain Ends at the Crystallite Surface

125-character teaser:

Polymer chain ends mostly confined to crystallite surfaces have been detected by versatile isotope labeling and advanced NMR.

Authors

Shichen Yuan¹, Klaus Schmidt-Rohr^{1*}

*Corresponding author. Email: srohr@brandeis.edu

Affiliations

¹ Department of Chemistry, Brandeis University, Waltham, MA 02453, USA

Abstract

A comprehensive ^{13}C NMR approach for characterizing the location of chain ends of polyethers and polyesters, at the crystallite surface or in the amorphous layers, is presented. The OH chain ends of polyoxymethylene have been labeled with ^{13}COO -acetyl groups and their dynamics probed by ^{13}C NMR with chemical-shift-anisotropy (CSA) recoupling. At least 3/4 of the chain ends are not mobile dangling cilia but are significantly immobilized, exhibiting a powder pattern characteristic of the crystalline environment as well as fast CSA dephasing. The location and clustering of the immobilized chain ends has been analyzed by spin diffusion. Fast ^1H spin diffusion from the amorphous regions shows confinement of most chain ends to the crystallite surface, confirmed by fast ^{13}C spin exchange between ^{13}COO chain ends. These observations confirm the principle of avoidance of density anomalies, which requires that chains terminate at the crystallite surface in order to stay out of the crowded interfacial layer.

Introduction

Chain ends can play an important if underappreciated role in the formation and stability of the lamellar semicrystalline morphology of many polymers (1). Fig. 1 displays four distinct potential distributions of chain ends that have been shown in the literature for five decades but could not be distinguished experimentally except in the special case of polyethylene. While it was speculated early on (2) that dangling cilia (see Fig. 1a) of otherwise tightly folded chains give rise to the ~15% mobile amorphous segments almost ubiquitously observed in polymers of high crystallinity, including solution crystals, such structural models often produce crowded interfacial layers with excess density higher than in the crystallites (1, 3, 4). Such a density anomaly, which arises as chains leave a densely packed crystallite and meander in the disordered interfacial layer, impinging on each other (1), is significantly reduced if chains are not only tilted relative to the crystallite surface normal (1, 3, 5) but also terminate at the crystallite surface so that they avoid entering the crowded interfacial layer (Fig. 1b) (1). Chain ends are indeed concentrated at the lamellar surface in monodisperse oligomeric systems, e.g. long chain n-alkanes (6) and polyethylene oxide (PEO) (7), after transient non-integer folding has transformed into stable integer folding. A majority of chain ends immobilized at the surface of the crystallites in polydisperse polyethylene (PE) have been detected by $^{13}\text{C}\{^1\text{H}\}$ and ^2H solid-state NMR (1, 8). Furthermore, with decreased concentration of chain ends due to increased molecular weight, crowding

47 reduction in the interfacial layer requires more pronounced chain tilt relative to the shortest trajectory through the
48 crystallite (1, 9).

49
50 Chain ends can reach their thermodynamically favored locations if the chains are sufficiently mobile either during
51 crystallization or in the solid state due to α_c mobility (chain diffusion) (10-12), which also enables solvent-free PE
52 processing (13). In crystal-fixed polymers (11), chain ends might be trapped throughout the crystallites. Then, an
53 approximately homogeneous distribution of polymer chain ends throughout the crystalline regions (14) should lead to
54 row defects (Fig. 1c) or significant disorder in the crystallites (Fig. 1d). To date, most studies of the chain end
55 distribution have focused on PE, an α_c -mobile polymer, and found evidence for the structural features of Fig. 1b (1,
56 6, 8). Whether other polymers with different chain mobility, chain conformation (1), interchain interactions (15) or
57 crystallization kinetics (12, 16) exhibit different chain-end distributions is not known.

58 Studies of the spatial distribution of chain ends have been limited (1, 8, 14, 17), probably due to the experimental
59 difficulties associated with the low concentration of chain ends. The NMR studies have been based on well-resolved
60 end-group signals (1, 14) or specific block-copolymer synthesis (8) particular to PE, which do not generalize to other
61 polymers. Therefore, the development of new approaches to characterize other types of chain ends is desirable. In this
62 study, we analyze chain ends in polyoxymethylene (POM), a relatively hard engineering polymer which has very
63 slow chain diffusion at 298 K (18) as well as high crystallinity and might therefore have a different chain-end
64 distribution than PE. Via acetylation, the 'natural' OH chain ends in POM homopolymer can be converted into acetyl
65 groups, which is adopted in industry to prevent thermal degradation of POM (19, 20) and can be generalized to
66 polyesters and other polyethers. Acetyl groups are much less bulky than other chain-end tags such as the TEMPO
67 group for EPR studies (21) and therefore have no significant disruptive effect. By acetylation using ^{13}C -enriched
68 acetic anhydride, the small NMR signal of chain ends can be enhanced 90-fold.

69 In this work, we demonstrate how the distribution of ^{13}C -labeled acetylated chain ends across the semicrystalline
70 morphology can be studied by a series of state-of-the-art NMR techniques. Contrast in segmental mobility between
71 the nearly rigid crystallites and the mobile amorphous layers is exploited to distinguish chain ends in the crystallites
72 from those in the amorphous regions. The motional narrowing of C-H or H-H wide-line spectra (22, 23) commonly
73 exploited to characterize the motions of CH_2 or CH groups cannot be used here, but for the ^{13}C -enriched esters the
74 chemical-shift anisotropy (CSA) is a good probe of mobility (24). Motional narrowing of CSA powder patterns can
75 be detected with isotropic-shift resolution in two-dimensional separation of undistorted powder-patterns by effortless
76 recoupling (SUPER) (25) NMR spectra, while quantification of the mobile chain end fraction is enabled by CSA-
77 dephasing NMR (26) after direct polarization. The spectrally resolved immobilized crystalline and mobile amorphous
78 backbone esters in unlabeled poly(ϵ -caprolactone), PCL, are analyzed for reference. Selective detection of end groups
79 with limited mobility is achieved by ^1H -double quantum filtering (27) with ^{13}C detection. The depth of the chain ends
80 from the crystallite surface can be probed by ^1H spin diffusion (28) after a $T_{2\text{H}}$ and chemical-shift filter. The
81 clustering of chain ends at the crystallite surface can be detected by CODEX NMR (29) with ^{13}C spin exchange,
82 potentially even in the absence of amorphous-phase mobility. Some properties of the crystallite surface can be probed
83 by analysis of the relative orientation of chain ends concentrated at that surface. The NMR methods demonstrated
84 here can be applied to characterize chain ends in other polyethers and in polyesters originally terminated with OH
85 groups.

86 87 88 **Results**

89 ***Crystallinity and ^{13}COO Fraction from Quantitative ^{13}C NMR***

90 A quantitative direct polarization (DP) ^{13}C NMR spectrum of ^{13}C -Ac₂-POM is shown as the top trace in Fig. 2.
91 Quantitative signal intensities were obtained with a recycle delay of 125 s, based on a $T_{1\text{C}}$ relaxation time of 20 s in
92 POM (Fig. S2) (30). The spectrum shows two peaks, one from the ^{13}C -enriched ester groups of the acetyl chain ends,
93 the other due to ^{13}C in natural abundance in the O-CH₂-O units of POM. The peak ratio of 1.04:1, combined with the
94 isotopic-enrichment factor of 99%/1.1%, yields a concentration of one ^{13}COO end group per 94 O-CH₂ units. This
95 corresponds to a number-average molecular weight of $M_n = 4.7$ kg/mol if $\geq 90\%$ acetylation of chain ends is assumed.
96 The strong end-group signal in Fig. 2 demonstrates that even with a five-times higher molecular weight M_n , the end-
97 group signal strength would be sufficient to be detectable by NMR.

98 The signal of mobile $^{13}\text{CH}_2$ groups in the amorphous regions of POM can be selected by direct polarization with a
99 short recycle delay, since fast ^{13}C spin-lattice ($T_{1\text{C}}$) relaxation is driven by fluctuating CH dipolar fields with spectral
100 density near the ^{13}C Larmor frequency. The amorphous O-CH₂-O signal quantitatively selected using a recycle delay
101 of 0.5 s is shown as the bottom trace in Fig. 2, normalized per scan. The fractional area of the broad O-CH₂-O band
102 (between 85 and 95 ppm, see Fig. S3) corresponds to an amorphicity of 0.3 and thus a crystallinity of 0.7.

Analysis of Immobilization of Chain Ends by Chemical Shift Anisotropy Recoupling

Solid-state NMR can easily probe the fast, large-amplitude motions that chain ends in dangling cilia (Fig. 1a) would be expected to undergo, in terms of spectral line narrowing. While for CH_n segments motional narrowing of C-H or H-H wide-line spectra (22, 23) can be observed conveniently, for ester groups the chemical-shift anisotropy, producing a broad, well-defined powder pattern (28, 31) in the rigid limit, is a particularly good probe of mobility (24). A potentially motionally narrowed CSA powder pattern can be obtained for each resolved peak in the MAS ^{13}C NMR spectrum using two-dimensional separation of undistorted powder-patterns by effortless recoupling (SUPER)(25). To demonstrate the rigid-limit ester powder pattern as well as motional narrowing due to large-amplitude motions, Fig. 3a presents the comparison of patterns extracted from CP-based and DP-based SUPER spectra of the semicrystalline polyester poly(ϵ -caprolactone), PCL. The characteristic, broad ester CSA powder pattern at the crystalline resonance (173.6 ppm) of PCL was extracted from a 2D SUPER spectrum (see Fig. S4a) after cross polarization from ^1H , while the motionally narrowed peak at the amorphous ester resonance (172.8 ppm) was obtained after direct polarization with short recycle delay. The contrast between the two spectra confirmed that rigid and mobile segments can be separated through CP-based and short-DP-based experiments, respectively. Fig. 3b displays CSA powder patterns of the rigid and partially mobile chain ends in ^{13}C -Ac₂-POM, extracted from CP-based and short-DP-based SUPER ^{13}C NMR spectra, respectively (see Fig. S4b for contour plots of the two-dimensional spectra). The broad, well-defined powder pattern of the chain ends extracted from the CP-based SUPER spectrum spans essentially the same range as the pattern of the PCL crystallites, showing no evidence of fast large-amplitude motions. Even after 0.5 s direct polarization, which selects signals of the most mobile segments as demonstrated for PCL, only a small fraction of end groups produce a narrow peak at the isotropic chemical shift (marked by a dashed vertical line), while most still exhibit significant residual anisotropic broadening, which excludes fast isotropic motions even for these more mobile POM end groups.

Quantification of the immobilized chain-end fraction is best achieved in terms of relative peak areas in mobility-selective but otherwise quantitative one-dimensional NMR spectra. For CH_n groups in polymers, selective spectra of mobile segments can be obtained by several relaxation-based solid-state NMR techniques, including direct polarization with short recycle delay as demonstrated above. However, the acetyl chain-end ^{13}COO carbon has weak dipolar couplings to protons, which makes $T_{1\text{C}}$ and T_{CH} relaxation of mobile segments less distinctive. On the other hand, the much larger CSA of rigid crystalline COO segments compared to highly mobile esters can be exploited in a CSA filter (26), which suppresses the rigid while retaining the mobile-COO signals because the apparent transverse relaxation time is inversely proportional to the width of the CSA powder spectrum. While in regular magic-angle spinning the CSA effect is time-averaged to zero, during a CSA filter it is recoupled by three rotation-synchronized π -pulses that interfere with its averaging by MAS (26).

For reference, Figs. 3c and 3d demonstrate the effect of a CSA filter with a 32 μs spacing of the first two π -pulses on the COO segments in crystalline (173.8 ppm, polarized by 1.1 ms CP) and amorphous (172.8 ppm, polarized by DP with 1 s recycle delay) components in PCL, respectively. For rigid COO groups detected after CP, complete suppression of signal intensity is observed (CSA-filtered signal S in Fig. 3c). Conversely, most magnetization of mobile COOs polarized by 1 s DP passes the 32 μs CSA filter and $\sim 88\%$ of the amorphous COO peak remains (see Fig. 3d). The observed dramatic differences between CP-based and DP-based spectra confirm that only mobile COO groups can survive the CSA filter.

The same 32 μs CSA filter proven to effectively dephase the rigid ester signal was applied to ^{13}C -Ac₂-POM after DP with a 70 s recycle delay, as demonstrated in Fig. 3e. Since $T_{1\text{C}}$ of chain-end COO, driven by the fluctuating fields of the nearby rotating acetyl methyl group, is ~ 7 s, DP with a 70 s recycle delay can comprehensively polarize chain-end COO groups in both crystalline and amorphous regions with negligible bias. Fig. 3e shows the COO signal obtained with (S) and without (S_0) 32 μs CSA filtering. The ratio of S/S_0 , representing the mobile COO chain-end fraction, is $\sim 25\%$. This leads to the conclusion that about 75% of the chain ends are immobilized.

Signals of Immobilized Segments by Quasi-static ^1H DQ Filtering

Selection of signal of chain ends with little mobility, complementary to CSA filtering, can be achieved by ^1H quasi-static double-quantum (DQ) filtering at 4 kHz MAS. For rigid CH_2 groups, the strong ^1H - ^1H dipolar couplings quickly generate two-spin coherences that can be converted to double-quantum coherences and selectively back to ^1H magnetization, whereas the motionally averaged dipolar couplings of highly mobile segments are too weak to generate such coherences in the given short time. With only $2 \times 6 \mu\text{s}$ of ^1H homonuclear dipolar double-quantum coherence excitation and reconversion, chemical-shift evolution and the change in rotor orientation can also be neglected. Through short 0.4 ms cross polarization, the magnetization of the rigid ^1H - ^1H spin pairs is transferred to nearby chain-end COO groups. A more extensive discussion of the pulse sequence can be found in the SM.

Figs. 4a and 4b demonstrate the successful selection of ^1H magnetization of immobilized CH_2 groups and suppression of signals of mobile segments in branched PE and in PCL, two semicrystalline polymers with significant amorphous

161 fractions. The amorphous methylene signals at 31.0 ppm and 64.2 ppm, respectively, detected in the quantitative
162 spectra (top traces) and the 0.4 ms CP spectra (middle traces) are almost completely suppressed by applying the 2×6
163 μs quasi-static DQ filter (bottom traces). These results confirm that the quasi-static DQ filter can select the ^1H
164 magnetization of CH_2 groups in a rigid crystalline environment.

165 The spectrum of ^{13}C -Ac₂-POM after $2 \times 6 \mu\text{s}$ quasi-static ^1H DQ filtering and cross polarization is shown as the
166 bottom-trace (red line) in Fig. 4c. About 41% of the intensity of the broad amorphous O-CH₂-O band is seen to be
167 suppressed (see Fig. S3c-e for a deconvolution analysis), which indicates that only a limited fraction of the O-CH₂-O
168 segments in the amorphous layer are highly mobile. The relative intensities of the COO signals near 170 ppm show
169 that of all the chain-end esters that are cross-polarizable, $\sim 75\%$ are in a sufficiently immobile environment to pass
170 the quasi-static DQ filter, which is consistent with the immobile fraction of $\sim 75\%$ deduced from CSA dephasing.

171 ***Probing the Distribution of Chain Ends across the Crystals by ^1H Spin Diffusion***

172 The distribution of chain ends in the crystallites can be probed by ^1H spin diffusion (28) from the amorphous to the
173 crystalline regions. If the chain ends were uniformly distributed throughout the crystallites, as in Figs. 1c/d, their
174 signal would recover by spin diffusion in parallel with that of the crystalline O-CH₂-O groups. On the other hand, if
175 chain ends are localized at the crystallite surface as in Fig. 1b, they are reached earlier by the magnetization transfer
176 from the amorphous regions and their signals reappear earlier. The magnetization level change at the crystallite
177 surface is particularly distinct from that in the bulk of the crystallite if the amorphous source fraction is $< 50\%$, as is
178 the case in POM: Not only does the magnetization at the crystallite surface initially increase quickly, but it later also
179 drops as the magnetization drains into the interior of the crystallite. A resulting maximum (32) is characteristic of
180 segments at the crystallite surface.

181 To start off the spin diffusion experiment with ^1H magnetization only in the mobile O-CH₂-O segments, a $T_{2\text{H}}$ filter of
182 200 μs duration (32) can be applied on-resonance; it also serves as a chemical-shift filter to suppress the
183 magnetization of the acetyl CH_3 groups, which may otherwise be incompletely suppressed because they undergo fast
184 rotational jumps that increase their $T_{2\text{H}}$ relaxation time. ^1H spin-diffusion from the selected amorphous to the rigid
185 components occurs during the spin-diffusion time t_{SD} after the $T_{2\text{H}}$ filter and before cross polarization to ^{13}C . After the
186 shortest spin-diffusion times ($t_{\text{SD}} < 0.11$ ms), only the characteristic broad line shape of the amorphous O-CH₂-O
187 segments near 90 ppm is observed, see Figs. 5a and S3b, which confirms successful selection of magnetization in the
188 noncrystalline regions. Increasing t_{SD} allows for the transfer of ^1H magnetization to the crystalline component as well
189 as a corresponding loss of ^1H magnetization in the amorphous component. Consequently, the sharp crystalline O-
190 CH₂-O peak gradually reappears while the intensity of the broad O-CH₂-O band decreases. Asymptotic values are
191 reached within 50 ms. The spectra at long spin diffusion times of ≥ 100 ms are identical to the line shape of the
192 unselective CP spectrum, indicating full equilibration of the magnetization by the spin-diffusion process. Fig. 5b
193 summarizes the time evolution of the intensity of the chain-end ^{13}COO and the deconvolved crystalline O-CH₂-O
194 signals as a function of the square root of the spin diffusion time, since this results in nearly linear initial increases.
195 The vertical scaling in the figure gives the magnetization per ^1H spin, with the equilibrium level of 0.22 (the
196 estimated mobile amorphous fraction selected by the $T_{2\text{H}}$ filter, see also Fig. S6).

197 The build-up of the chain-end COO signal with t_{SD} is characteristically different from that of the crystalline O-CH₂-O
198 peak. It exhibits a fast increase with t_{SD} in the initial spin-diffusion process, reaches a maximum at $t_{\text{SD}} \sim 1$ ms, and
199 then gradually decreases to the equilibrium level at $t_{\text{SD}} \geq 10$ ms. The initial buildup rate of signal of immobilized
200 chain ends ($\sim 0.25 \text{ ms}^{-1/2}$) is much larger than that of the crystallite peak ($\sim 0.06 \text{ ms}^{-1/2}$), which indicates that most of
201 the immobilized chain ends are spatially close to the amorphous regions, i.e. concentrated at the crystallite surface.
202 Simulations of the spin diffusion after the $T_{2\text{H}}$ filtering can provide more insight into the width of the surface chain-
203 end distribution. Using a spin-diffusion model with amorphous, surface, and crystalline layer thicknesses of 1.75 nm,
204 0.25 nm, and 6.25 nm, respectively (simulation details can be found in the SM), the simulated buildup for surface
205 COO and crystalline O-CH₂-O fit the experimental data. The pronounced maximum in COO-group magnetization can
206 only be reproduced if the immobilized ^{13}COO chain ends are concentrated in a thin layer at the crystallite surface.
207

208 ***Close Contacts among Chain Ends Detected by ^{13}C CODEX NMR***

209 Clustering of ^{13}COO chain ends at the crystallite surface can be probed by CODEX ^{13}C NMR with dipolar ^{13}C spin
210 exchange (29). CODEX can detect magnetization transfer between ^{13}C spins in differently oriented, magnetically
211 inequivalent COO segments. Dipolar-driven spin exchange occurs faster the closer the ^{13}COO groups, due to the
212 strong distance dependence of the ^{13}C - ^{13}C dipolar couplings (33). Chain ends that concentrate at the crystallite
213 surface introduce closer contacts among ^{13}COO groups than if the ^{13}COO groups were uniformly distributed in the
214 bulk, thereby resulting in relatively fast ^{13}C - ^{13}C spin exchange. Such spin exchange can be detected in CODEX
215 experiments (29), where ^{13}C magnetization dephased by CSA recoupling will not refocus into a stimulated echo after
216 the mixing time if spin exchange to a ^{13}C site with a different segmental orientation has occurred.

For ^{13}C -Ac₂-POM, the normalized CODEX signal S/S_0 of chain-end ^{13}COO groups as a function of the mixing time t_m is shown in Fig. 6a. This represents the fraction of chain-end ^{13}C magnetization retaining the same orientation-dependent chemical shift after spin exchange for a time t_m . Spin exchange between magnetically inequivalent ^{13}COO groups driven by dipolar couplings leads to a pronounced decay of S/S_0 as a function of t_m , if the CSA dephasing and refocusing time Nt_r is sufficiently long. The S/S_0 values with $Nt_r = 1.2$ ms and 2.4 ms were similar, indicating that the asymptotic limit (29) has been reached within the 1.2 ms of CSA recoupling used in the experiments. The S/S_0 ratio decays very fast initially as a function of t_m , with a rate of ca. 0.7 s^{-1} , which indicates close contact among magnetically inequivalent ^{13}COO end groups. Additionally, S/S_0 decays to as low as 0.3 within a mixing time of 5 s, which indicates that more than two other magnetically inequivalent sites are nearby (29). To confirm that the decay is caused by spin exchange instead of molecular motion, two additional series of CODEX experiments were performed at higher MAS frequencies of 12.5 kHz and 20 kHz. While the CODEX decay would stay unchanged if the exchange was due to motions, dipolar exchange is slowed down by faster MAS (34). Fig. S7 shows the experimental decays at 5, 12.5, and 20 kHz MAS. With increasing MAS frequency and constant $Nt_r = 0.8$ ms, the S/S_0 decay was considerably slowed down, proving that the exchange process at 5 kHz MAS is dominated by dipolar spin exchange. It can therefore be analyzed using spin-exchange theory as discussed below.

Discussion

Immobilized Chain Ends at the Crystallite Surface

Cartoons like those in Fig. 1 have been shown in the literature for over fifty years, but experimental data confirming them or ruling them out have been scarce. The current study has shown various lines of evidence that ~75% of chain ends in POM are essentially immobilized at the crystallite surface. Since T_g of POM is ~70 K below room temperature, chain ends terminating in flexible cilia in the amorphous region as depicted in Fig. 1a should be highly mobile. They should then give rise to a narrow peak like the CSA line shape extracted from short DP-based SUPER experiments (see Fig. 3a), would not be expected to produce signal after a short DQ filter, and during spin-diffusion out of the mobile regions their signal should consistently decrease. However, the data from the mobility filtering experiments show none of these behaviors, revealing that most chain ends are not mobile. While the ^{13}C -Ac₂-POM for which the new approach was demonstrated here has only a rather small and inconspicuous mobile amorphous layer, the incorporation of the ester groups into an immobilized solid-like environment observed here does show that the end group is not forced into the most mobile amorphous layer. Both ^1H and ^{13}C spin-diffusion experiments show strong evidence of immobilized chain ends concentrated at the surface of the crystalline regions, which agrees with the schematic presented in Fig. 1b.

Probing the Spatial Distribution of Chain Ends by ^1H and ^{13}C Spin Diffusion

Simulations of ^1H spin diffusion in Fig. 5b show that the observed chain-end build-up behavior can only be matched if immobilized chain ends are mostly concentrated in a thin layer at the crystallite surface. The simulations shown in Fig. 5b indicate amorphous, surface, and crystalline layer thicknesses of 1.75 nm, 0.25 nm, and 6.25 nm, respectively. With a long period of ~ 8.5 nm from SAXS (Fig. S1) and a chain contour length of ~ 30 nm based on the chain-end concentration, a typical chain traverses a crystallite approximately three times. It therefore crosses the interface six times, out of which two can correspond to ^{13}COO chain ends (I). The resulting chain-end concentration at the crystallite surface would be up to about $2/6 = 33\%$.

According to the crystal structure of POM, in the absence of chain tilt all segments at the crystallite surface have the same orientation and therefore the same NMR frequency (see Fig. S9a). Since CODEX reflects frequency change due to spin exchange, without chain tilt no significant CODEX decay would be observed for chain ends at the crystallite surface, in striking contrast with the experimental results. Otherwise put, the CODEX data indicate chain tilt relative to the local lamellar normal (see Fig. S9b), which is in agreement with a ~30° tilt angle of POM chains observed after roll-milling (35). Note that the anisotropic chemical shift in the CODEX experiment does not specifically probe the chain-axis direction but would change if the POM helix was rotated around its axis (18). Thus, the different chain ends in Fig. 1b would mostly have different frequencies.

The observed initial CODEX dephasing in Fig. 6a is surprisingly fast, indicating many close approaches among ^{13}COO end groups. A detailed inspection of the POM unit cell shows that the closest inter-stem ^{13}C - ^{13}C contact is ~ 3.7 Å for two adjacent stems on the (1 0 0) face (the crystal growth front (36)). A crystallite surface cleaved along a (2 $\bar{1}$ 14) plane contains the closest inter-stem ^{13}C - ^{13}C pair and matches the chain tilt as well as crystal-growth face conditions. For ^{13}COO chain ends in such a (2 $\bar{1}$ 14) plane, simulations of ^{13}C - ^{13}C spin exchange were performed with various ^{13}COO chain-end fractions ranging from 100% (all segments at the crystallite surface are chain ends) to 10%; details on the CODEX simulations can be found in the SM. The resulting decay curves are presented in Fig. 6a. The best agreement is obtained for 25% to 33% ^{13}COO chain ends randomly distributed in the plane, see Fig. 6b. This is consistent with the value of $2/6 = 33\%$ chain ends at the crystallite surface obtained for a typical POM chain

273 passing through the crystallite three times, if one takes into account the ~25% chain ends in the amorphous core layer,
274 which correspondingly reduces the chain-end fraction at the crystallite surface.

275 The model in Fig. 6b may seem to lack the roughness of crystallite surfaces observed experimentally (37). We
276 propose that chain ends are only moderately disordered because we attribute the roughness mostly to the complex
277 connectivity of chains across the crystalline–noncrystalline interface, resulting in tight folds for adjacent reentry,
278 loops for nonadjacent reentry, entangled loops, tie molecules, crowding problems (1), etc. Chain ends at the
279 crystallite surface are not subject to any of these disorder-inducing connectivity effects. We expect neighboring chain
280 ends, which are probed by the CODEX NMR experiment, to be all found near the local crystallite surface since this
281 avoids formation of vacancies. The close approaches between chain ends and their sharp depth profile observed here
282 are inconsistent with significant random chain-end displacements into and out of the crystallite that would be
283 associated with surface roughness involving chain ends. The data also clearly exclude dispersal of a significant
284 fraction (>10%) of chain ends throughout the crystal as in Figs. 1c/d.
285

286 ***The Chain-End ¹³C-Acetylation Approach***

287 The functionalization of polymer chain ends with strong-signal tags presented here overcomes the low signal-to-noise
288 ratio that has been the main hurdle to the characterization of these low-concentration species. The approach is simpler
289 than previous chain-end chemical modifications, some of which required demanding chemical reactions (e.g. anionic
290 polymerization of isotopically labeled monomers (8, 38)). Other end groups giving strong signals, such as stable-
291 radical (TEMPO) end caps, are too bulky to fit into the crystalline lattice (21). The acetyl end group used here, first
292 introduced as a chain-end stabilizer for POM (19), is not only small enough to be considered as a regular chain end,
293 but is also chemically convenient to produce. It has long been used in industrial polymers without significant
294 detrimental effects on physical properties. Our data indicate that chain-end ¹³COO labeling enables the
295 characterization of properties of chain ends by a series of solid-state-NMR techniques with adequate signal-to-noise
296 ratio for number-averaged molecular weights exceeding 30 kg/mol. The approach can be applied to other polyethers
297 as well as to polyesters.

298 ***Conclusions***

299 An approach combining ¹³C-labeling of chain ends and a variety of modern NMR experiments for probing the
300 distribution of the chain ends in the semicrystalline morphology has been demonstrated in POM. The convenient ¹³C-
301 labeling scheme via acetylation is also applicable, with minor variations, to other OH-terminated polymers, which
302 include not only other polyethers but also polyesters. The hypothesis of dangling chain ends or cilia of otherwise
303 tightly folded chains giving rise to the ~15% mobile segments in highly crystalline homopolymers, previously
304 falsified for high-density polyethylene, has been disproved here again, in a different polymer. The chemical-shift
305 anisotropy powder patterns and dephasing data demonstrate the spectral characteristics of nearly immobilized chain
306 ends, which provides a useful reference for other polymers with highly mobile acetyl chain ends, as observed in
307 ongoing studies in our laboratory. The location of the chain ends at the crystallite surface was documented by an
308 unusual maximum in the chain-end magnetization as a function of ¹H spin diffusion time. The clustering of the ¹³C-
309 labeled chain ends resulting from their confinement to thin layers at the crystallite surfaces was confirmed by fast and
310 extensive ¹³C-¹³C spin exchange detected by CODEX NMR. The present study demonstrates that even when
311 crystalline and noncrystalline acetyl chain ends do not exhibit a significant chemical-shift difference, modern
312 mobility- and spin-diffusion-based NMR can identify and quantify crystal-immobilized chain ends. A better
313 understanding of the distribution of chain ends promises to shed more light on the crystallization process of semi-
314 crystalline polymers.
315

316 ***Materials and Methods***

317 ***Materials***

318 1,3,5-trioxane (99%), n-hexane, N,N-dimethylcyclohexylamine, and poly(ε-caprolactone) (PCL, $M_n = 10$ kg/mol)
319 were purchased from Sigma-Aldrich; methanol, acetone, unlabeled palmitic acid from Fisher; acetic anhydride (1,1'-
320 ¹³C, 99%) and 1-¹³C-palmitic acid from Cambridge Isotope Laboratories; calcium hydride (93%) from Acros
321 Organics; and boron trifluoride diethyl ether (98+%) from Alfa Aesar. The branched polyethylene (hydrogenated
322 polybutadiene) with $M_n = 15$ kg/mol has been described in Ref (39).

323 ***Synthesis of POM***

324 1,3,5-trioxane was purified by sublimation under atmospheric pressure at 50 °C. The resulting needle crystallites (0.5
325 g) were transferred into a 50 mL oven-dried flask containing 25 mL of n-hexane dried over CaH₂ reflux, which was

326 sealed using a rubber septum. Trioxane crystallites were fully dissolved by heating the solution to 50 °C under
327 atmospheric pressure (using a dry-air balloon), which was followed by injecting 0.1 mL BF₃-etherate n-hexane
328 solution (0.1 M) through septa while shaking. After a short period of time, the atmosphere above the solution became
329 cloudy. The solution was then kept at 45 °C for 12 h, allowing the polymerization to complete. The residual cations
330 in the POM samples were quenched by boiling with and precipitation from acetone twice (each time for 20 min). The
331 final product was filtered and dried in a fume hood overnight at room temperature (20).

332 **Chain-End Acetylation**

333 Polyoxymethylene powder (0.1 g), together with 0.2 mL of 1-¹³C-(acetic anhydride), and 60 μL of N,N-
334 dimethylcyclohexylamine were frozen, then flame sealed under vacuum in a glass ampoule, heated to 200 °C to form
335 a melt, and kept at 180 °C for the acetylation reaction to occur for 30 min. The melt was gradually brought to room
336 temperature. The solidified product in the ampoule was dissolved in methanol to react with an excess amount of the
337 ¹³COO-labeled acetic anhydride. The precipitated powder was filtered out and washed twice with methanol. The
338 remaining white powder was then boiled with acetone for 1 h while stirring and filtered off under suction until the
339 polymer was odorless (19). The white powder product was dried overnight in a fume hood and kept in a desiccator
340 with K₂CO₃ for 1 day before being packed into a Kel-F insert of a 4 mm outer-diameter MAS rotor. This material is
341 termed ¹³C-Ac₂-POM in this paper. For CODEX NMR at several different spinning frequencies, the ¹³C-Ac₂-POM
342 sample was transferred to a 2.5 mm rotor. The same acetylation procedure was repeated with regular (unlabeled)
343 acetic anhydride to give the Ac₂-POM sample used in SAXS measurements.

344 **Small Angle X-ray Scattering**

345 A transmission SAXS measurement on Ac₂-POM was conducted using the Pilatus3R 300 K detector on the
346 SAXSLAB instrument at MIT. The X-ray wavelength was $\lambda(\text{CuK}\alpha_1) = 1.54 \text{ \AA}$, generated with full power of 45 kV
347 and 0.66 mA. The sample-to-detector distance was 459.1 mm. The sample was sealed in a quartz capillary and the
348 measurement was taken at room temperature for 5 min.

349 **NMR**

350 Experiments were performed using a Bruker Avance Neo 400WB NMR spectrometer at a ¹³C resonance frequency of
351 100 MHz. Most of the measurements were conducted using a Bruker double resonance magic-angle-spinning (MAS)
352 probe with 4 mm zirconia rotors. The ¹³C-Ac₂-POM sample was loaded in a Kel-F insert. The typical B₁ field
353 strength used in cross-polarization was 58 kHz and the rf field strength was 69 and 63 kHz for ¹H and ¹³C pulses,
354 respectively. Pulsed ¹H decoupling was applied during the echo and acquisition periods with field strengths of $\gamma B_1 / 2\pi$
355 = 95 kHz and 85 kHz, respectively. The typical recycle delays for CP-based experiments were 6 s, 6 s, 2 s and 20 s
356 for ¹³C-Ac₂-POM, PCL, PE (branched) and 1-¹³C-palmitic acid samples, respectively. ¹³C chemical shifts were
357 referenced to the α -¹³C-glycine COO resonance at 176.4 ppm. All NMR data were acquired at approximately 300
358 K. The MAS frequency for ¹³C-Ac₂-POM was 10 kHz unless otherwise noted.

359 For ¹³C direct polarization (DP) NMR experiments, recycle delays were set to 125 s with 512 scans, and 0.5 s with
360 16384 scans, for the quantitative spectrum and the spectrum of mobile CH₂ groups, respectively, of ¹³C-Ac₂-POM.
361 The Kel-F insert signal near 110 ppm was removed by subtracting the spectrum of an empty insert with the same
362 number of scans.

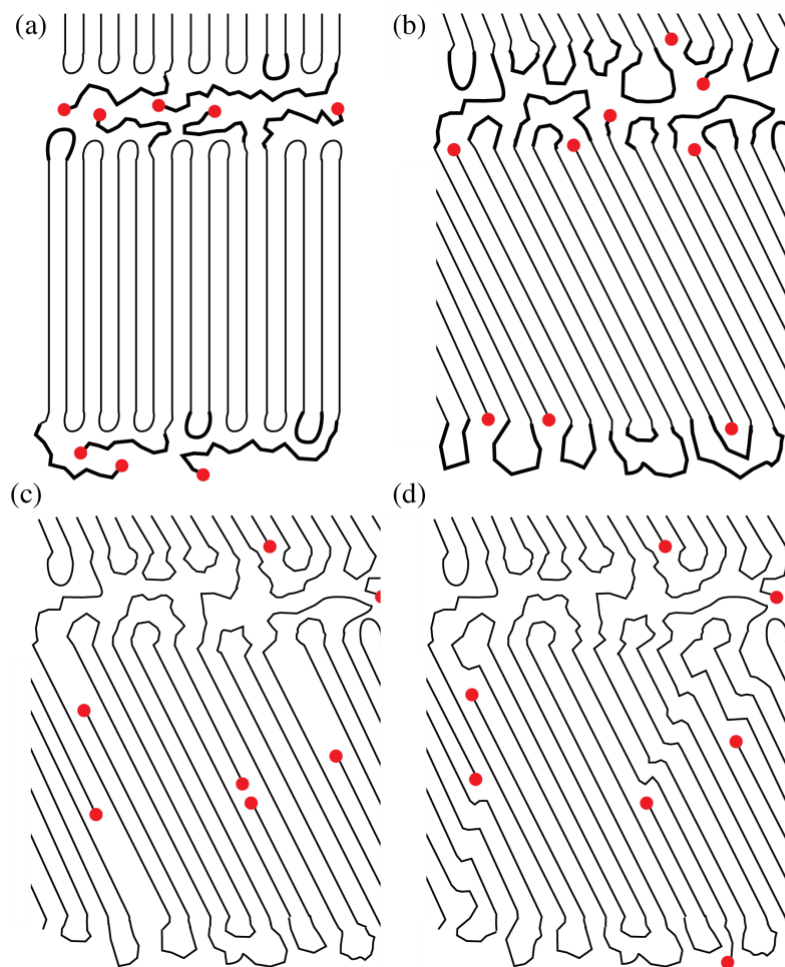
363 The separation of undistorted powder-patterns by effortless recoupling (SUPER) (25) experiments were conducted at
364 a MAS frequency of 5 kHz, after 0.4 ms CP or DP with a 1 s recycle delay, which selects rigid or mobile segments,
365 respectively.

366 For chemical-shift anisotropy (CSA) filtering with 3+2 pulses (26) at 10 kHz MAS, direct polarization with a 70 s
367 recycle delay was adopted to comprehensively excite the ¹³C magnetization of ¹³C-Ac₂-POM. For selecting rigid or
368 mobile segments of PCL, 1.1 ms CP or DP with a 1 s recycle delay, respectively, was used before the CSA filter. For
369 quasi-static ¹H double quantum (DQ) filtering with ¹³C detection, slow spinning at a MAS frequency of 4 kHz was
370 used to ensure that the 2 × 6 μs DQ generation and reconversion were applied to a barely rotated sample. The
371 detailed phase cycling in the pulse sequence (Fig. 4-inset) is listed in Table S1. Deconvolution of O-CH₂-O peaks
372 was performed using the MultiPeakFit package in iGor Pro 5.0.3 assuming Gaussian peak shapes. The amorphous
373 and crystalline peaks were determined from selective spectra and the CP spectrum, respectively, and the resulting
374 peak positions and widths were held fixed when deconvolving other spectra.

375 Experiments with ¹H spin-diffusion after T_{2H} filtering (Goldman-Shen experiment (40, 41)) and cross polarization to
376 ¹³C were used to detect the location of the immobilized chain ends relative to the crystallite surface. During the T_{2H}
377 filter of 200 μs duration, the C-H dipolar interaction was decoupled by irradiation at the ¹³C frequency with a field
378 strength of 43 kHz. The 200 μs evolution was also used as a chemical shift filter to suppress the ¹H magnetization of
379 the methyl groups in the acetyl chain ends, with the ¹H on-resonance frequency set to 4 ppm. The mixing time for ¹H
380 spin diffusion after the T_{2H} filter and before CP ranged from 10 μs to 300 ms.

381 The centerband-only detection of exchange (CODEX) (29) experiment was performed at a 5 kHz MAS frequency.
382 Mixing times between 10 ms and 5 s were utilized. The large CSA of chain-end COO and palmitic-acid COOH
383 groups enabled fast dephasing of magnetization in the evolution period. It was confirmed experimentally that $N_{tr} =$
384 1.2 ms (with $2 \times 5 \pi$ -pulses) and $N_{tr} = 2.4$ ms (with $2 \times 11 \pi$ -pulses) produced almost the same dephasing (long-time
385 limit).
386 To confirm that the origin of the fast CODEX dephasing in ^{13}C -Ac₂-POM was dipolar-driven spin exchange rather
387 than molecular motion (34), CODEX experiments were also performed in a double resonance probe with a 2.5 mm
388 zirconia rotor at MAS frequencies of 5, 12.5 and 20 kHz, with fixed $N_{tr} = 0.8$ ms. The ^{13}C 180° pulse length was as
389 short as possible, 5 μs , at MAS frequencies of 12.5 and 20 kHz, and correspondingly somewhat longer, 8 μs , at 5 kHz
390 MAS. The rf field strength for ^1H decoupling was 69 kHz.

391
392
393 **Acknowledgments:** SY would like to thank Bokai Xu and Prof. Isaac Krauss for kindly providing the initiator for the
394 polymerization, and Profs. Kay Saalwächter, Toshikazu Miyoshi and Bernard Lotz for helpful discussions.
395 **Funding:** The spectrometer used in this work was funded by the NSF MRI program, award No. 1726346.
396 **Competing interests:** The authors declare that they have no competing interests. **Author contributions:**
397 Both authors planned the project, executed NMR measurements, analyzed data, and wrote the manuscript.
398 SY synthesized ^{13}C -Ac₂-POM and performed CODEX and spin-diffusion simulations. **Data and materials**
399 **availability:** All data needed to evaluate the conclusions in the paper are present in the paper and/or the
400 Supplementary Materials. Additional data related to this paper may be requested from the authors.
401



403
 404
 405 **Fig. 1. Schematics of possible locations of chain ends (filled red circles) in the lamellar semicrystalline**
 406 **morphology.** Mobile segments (assuming $T \gg T_g$) are marked by a greater line thickness in (a, b). (a) Chain
 407 ends as dangling cilia. The location of the chain ends in low-density regions deep in the amorphous layers
 408 would facilitate their large-amplitude motions. (b) Chain ends mostly confined to the crystallite surface, in
 409 order to reduce excess density (I) in the folds and loops near the crystalline–amorphous interface. (c) Chain
 410 ends inside the crystallite generating row vacancy defects. A pair of chain ends are shown in the center of
 411 the figure. (d) Chain ends inside the crystallite producing kink defects. The crystallite thickness is typically 5
 412 – 30 nm (see also Fig. S1).
 413
 414
 415

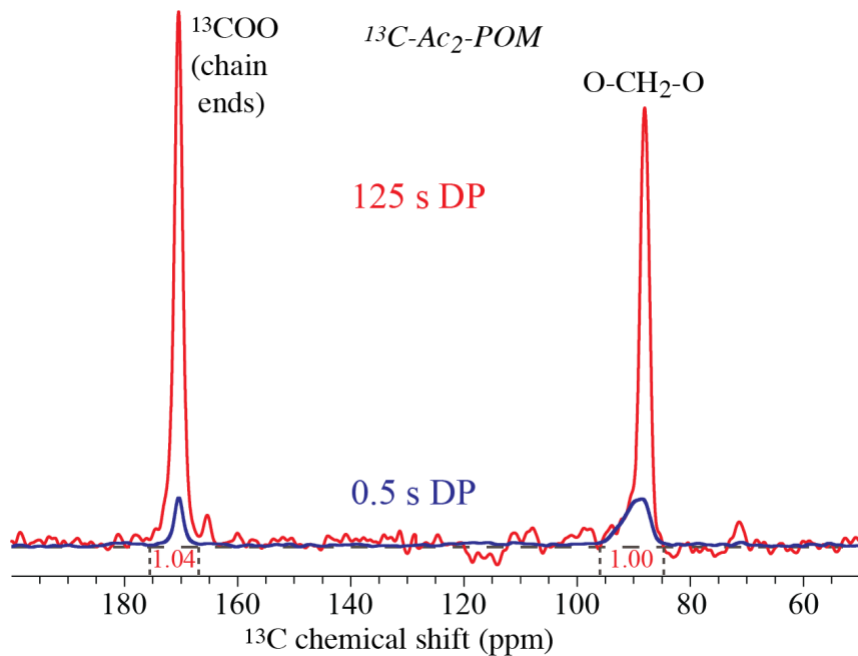


Fig 2. Direct polarization spectra of ^{13}C -Ac₂-POM. Top trace (red): Quantitative direct-polarization spectrum obtained with a 125 s recycle delay, with an integral ratio of $^{13}\text{COO} : \text{O-CH}_2\text{-O} = 1.04 : 1$; note that the chain-end signal is enhanced 90-fold by isotope labeling. Lower trace (blue): Selective direct-polarization spectrum of fast-relaxing, mobile O-CH₂-O segments obtained with a 0.5 s recycle delay.

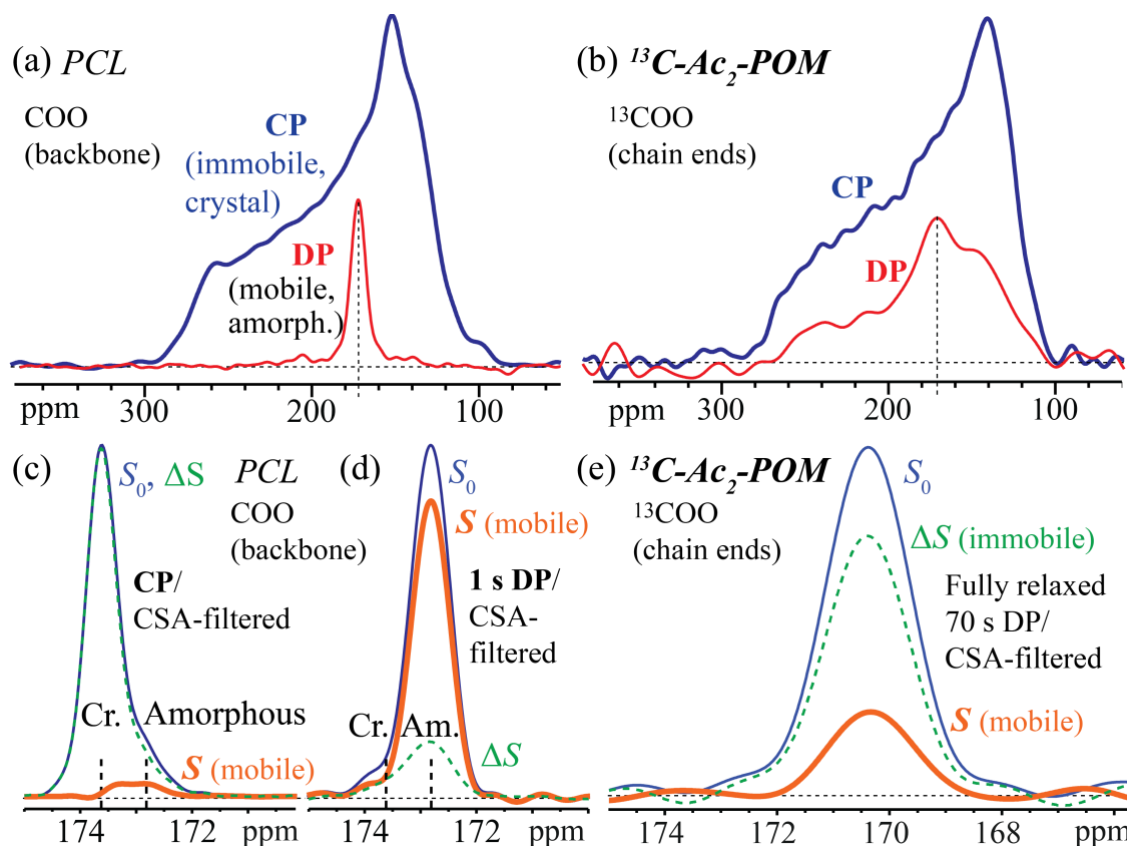
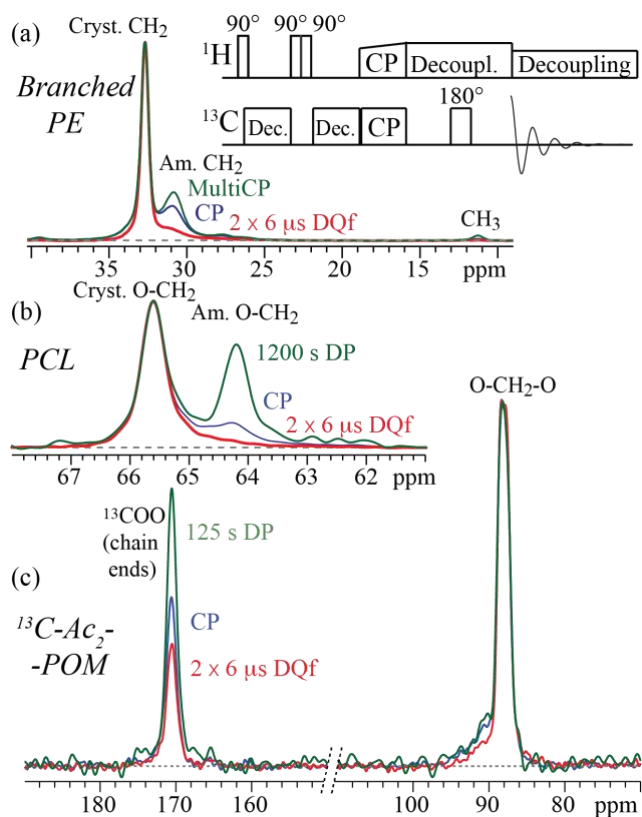
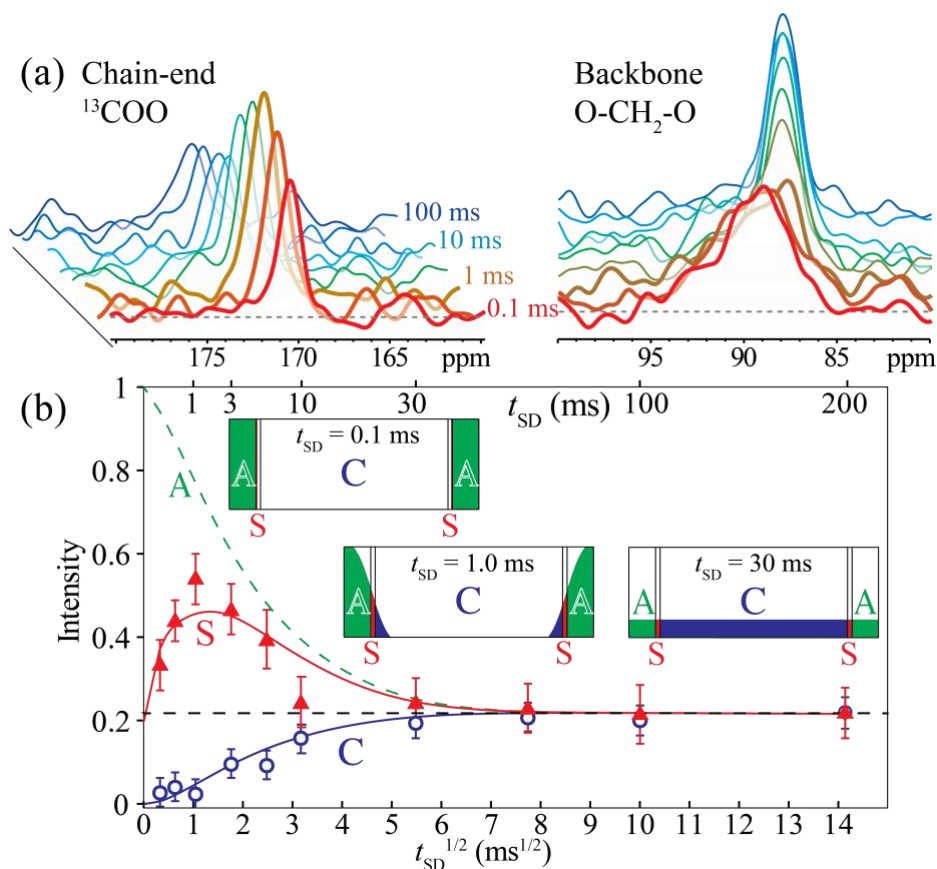


Fig. 3. Immobilized chain ends identified by chemical-shift anisotropy (CSA) recoupling. (a, b) ^{13}C CSA powder spectra of ester groups obtained by SUPER ^{13}C NMR after cross polarization (top traces, blue, solid-like) and 1 s direct polarization (bottom traces, red). (a) Spectra of the backbone esters in PCL shown for reference, extracted at

429 the crystalline (blue) and amorphous (red) resonance positions. (b) Spectra of the ^{13}C COO acetyl chain ends in ^{13}C -
 430 Ac_2 -POM. (c-e) Separation of ^{13}C NMR signals of immobile and mobile ester groups by a 3+2-pulse CSA filter (26)
 431 with a $32\ \mu\text{s}$ delay between first and second π -pulse. Thick orange line: Spectrum S after the CSA filter, from mobile
 432 segments with a motionally averaged small CSA. Thin blue line: Full spectrum (S_0) of all esters recorded with CSA
 433 dephasing. Dashed green line: Difference $S_0 - S$, mostly of esters with limited mobility. (c) Spectra of crystalline PCL
 434 selected by cross polarization. (d) Spectra of mobile, amorphous PCL selected by direct polarization with a 2 s
 435 recycle delay. (e) Comprehensive spectra of chain-end ^{13}C COO groups in ^{13}C - Ac_2 -POM with and without CSA
 436 filtering, after direct polarization with 70 s recycle delay (fully relaxed).
 437
 438

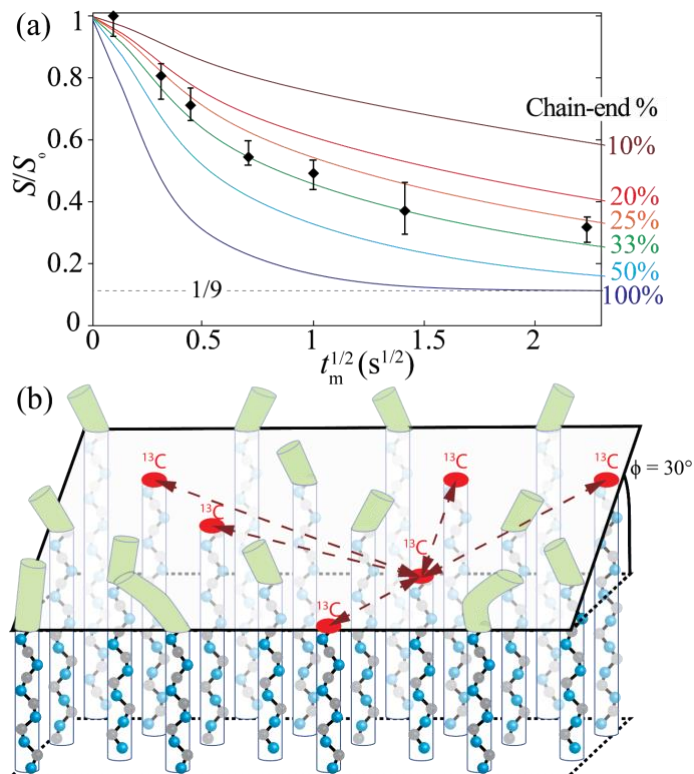


439
 440
 441 **Fig 4. Selection of signals of immobilized segments by quasi-static ^1H double-quantum filtering for $2 \times 6\ \mu\text{s}$,**
 442 **followed by 0.4 ms cross polarization to ^{13}C .** Spinning frequency: 4 kHz. The inset shows the pulse sequence; for
 443 details see the SM. (a, b) Demonstration of successful suppression of signals of mobile amorphous segments in (a) PE
 444 with 2.4 mol% ethyl branches and (b) PCL (O-CH_2 resonance). In addition to an unselective spectrum with the same
 445 CP time (blue middle trace), a quantitative DP or multiCP spectrum is also shown (green top trace in each figure). (c)
 446 Application to $^{13}\text{C-Ac}_2\text{-POM}$.



447
448
449
450
451
452
453
454
455
456
457

Fig 5. ^{13}C -detected ^1H spin diffusion from the amorphous regions in ^{13}C -Ac $_2$ -POM. (a) Series of spectra of the COO and O-CH $_2$ -O signals as a function of spin diffusion time, after 200 μs of $T_{2\text{H}}$ filtering that removes the crystalline ^1H magnetization and chemical-shift filtering that suppresses the CH $_3$ ^1H magnetization, at 10 kHz MAS. (b) Time evolution of the chain-end ^{13}COO resonance (filled triangles, top trace) and crystalline O-CH $_2$ -O resonance (open circles, bottom trace) as a function of the square root of the ^1H spin diffusion time. The curves show the simulated time dependences of magnetization in the amorphous (dashed), surface (red) and crystalline (blue) regions. The magnetization distribution at three time points is shown schematically in the insets, explaining the maximum of the surface magnetization at $t_{\text{SD}} = 1$ ms.



458
 459
 460 **Fig 6. Close contacts between chain ends in ^{13}C -Ac₂-POM detected by CODEX ^{13}C NMR with dipolar spin**
 461 **exchange.** (a) Normalized CODEX ^{13}C NMR signal (S/S_0) as a function of the square root of the ^{13}C spin-exchange
 462 mixing time ($t_m^{1/2}$), up to $t_m = 5$ s. A good fit of the CODEX decay is achieved with $\sim 30\%$ of the chains on the
 463 crystallite surface terminated by ^{13}C -Ac groups when the surface is a $(2\bar{1}14)$ face of the POM crystal (see the SM
 464 for simulation details). Since there are 9 distinct orientations of segments on the 9_5 helix of POM, the intensity at long
 465 t_m approaches $1/9$. (b) Schematic illustration of the distribution of chain ends (red) on a crystallite surface that is a
 466 $(2\bar{1}14)$ plane in the crystal structure of POM. The chains in the crystallite are tilted relative to the normal of the
 467 crystallite surface (black-outlined quadrangle). The chains continuing from the crystallite into the interfacial layer are
 468 indicated by green column segments close to the crystallite surface.

471
472
473
474
475
476
477
478
479
480
481
482
483
484
485
486
487
488
489
490
491
492
493
494
495
496
497
498
499
500
501
502
503
504
505
506
507
508
509
510
511
512
513
514
515
516
517
518
519
520
521
522
523
524
525
526
527
528
529
530
531

References

1. K. J. Fritzsche, K. Mao, K. Schmidt-Rohr, *Avoidance of Density Anomalies as a Structural Principle for Semicrystalline Polymers: The Importance of Chain Ends and Chain Tilt*. *Macromolecules* **50**, 1521-1540 (2017).
2. A. Keller, *Polymer crystals*. *Rep. Prog. Phys.* **31**, 623-704 (1968).
3. M. Hütter, P. J. in 't Veld, G. C. Rutledge, *Polyethylene {201} crystal surface: interface stresses and thermodynamics*. *Polymer* **47**, 5494-5504 (2006).
4. C. M. Guttman, J. D. Hoffman, E. A. DiMarzio, *Monte Carlo calculation of SANS for various models of semicrystalline polyethylene*. *Faraday Discussions of the Chemical Society* **68**, 297-309 (1979).
5. F. C. Frank, *General introduction*. *Faraday Discussions of the Chemical Society* **68**, 7-13 (1979).
6. G. Ungar, X. Zeng, *Learning Polymer Crystallization with the Aid of Linear, Branched and Cyclic Model Compounds*. *Chem. Rev.* **101**, 4157-4188 (2001).
7. S. Z. D. Cheng, J. Chen, A. Zhang, D. P. Heberer, *Nonintegral and integral folding crystal growth in low-molecular mass poly(ethylene oxide) fractions. II. End-group effect: α,ω -methoxy-poly(ethylene oxide)*. *J. Polym. Sci., Part B: Polym. Phys.* **29**, 299-310 (1991).
8. C. Wutz, M. J. Tanner, M. Brookhart, E. T. Samulski, *Where Are the Chain Ends in Semicrystalline Polyethylene?* *Macromolecules* **50**, 9066-9070 (2017).
9. R. G. Alamo, E. K. M. Chan, L. Mandelkern, I. G. Voigt-Martin, *Influence of molecular weight on the melting and phase structure of random copolymers of ethylene*. *Macromolecules* **25**, 6381-6394 (1992).
10. K. Schmidt-Rohr, H. W. Spiess, *Chain diffusion between crystalline and amorphous regions in polyethylene detected by 2D exchange ^{13}C NMR*. *Macromolecules* **24**, 5288-5293 (1991).
11. W. G. Hu, K. Schmidt-Rohr, *Polymer ultradrawability: the crucial role of α -relaxation chain mobility in the crystallites*. *Acta Polym.* **50**, 271-285 (1999).
12. K. Schäler, A. Achilles, R. Bärenwald, C. Hackel, K. Saalwächter, *Dynamics in Crystallites of Poly(ϵ -caprolactone) As Investigated by Solid-State NMR*. *Macromolecules* **46**, 7818-7825 (2013).
13. S. Rastogi, Y. Yao, S. Ronca, J. Bos, J. van der Eem, *Unprecedented High-Modulus High-Strength Tapes and Films of Ultrahigh Molecular Weight Polyethylene via Solvent-Free Route*. *Macromolecules* **44**, 5558-5568 (2011).
14. E. Pérez, D. L. Vanderhart, *Morphological partitioning of chain ends and methyl branches in melt-crystallized polyethylene by ^{13}C -NMR*. *J. Polym. Sci., Part B: Polym. Phys.* **25**, 1637-1653 (1987).
15. R. Kurz *et al.*, *Interplay between Crystallization and Entanglements in the Amorphous Phase of the Crystal-Fixed Polymer Poly(ϵ -caprolactone)*. *Macromolecules* **51**, 5831-5841 (2018).
16. M. Schulz *et al.*, *The Underestimated Effect of Intracrystalline Chain Dynamics on the Morphology and Stability of Semicrystalline Polymers*. *Macromolecules* **51**, 8377-8385 (2018).
17. A. Keller, D. J. Priest, *Experiments on the location of chain ends in monolayer single crystals of polyethylene*. *J. Macromol. Sci. Part B Phys.* **2**, 479-495 (1968).
18. A. P. M. Kentgens, E. de Boer, W. S. Veeman, *Ultraslow molecular motions in crystalline polyoxymethylene. A complete elucidation using two-dimensional solid state NMR*. *J. Chem. Phys.* **87**, 6859-6866 (1987).
19. N. M. Robert, 1956, Polyoxymethylenes, US2768994A.
20. D. Braun, H. Cherdrón, M. Rehan, H. Ritter, B. Voit, *Polymer Synthesis: Theory and Practice: Fundamentals, Methods, Experiments*. (Springer, 2004).
21. S. Hara, K. Yamamoto, S. Okamoto, S. Shimada, M. Sakaguchi, *Molecular Mobility of an Amorphous Chain in the Crystallization Process of Poly(ϵ -caprolactone)*. *Macromolecules* **37**, 5323-5326 (2004).
22. J. Schaefer, E. O. Stejskal, R. A. McKay, W. T. Dixon, *Molecular motion in polycarbonates by dipolar rotational spin-echo carbon-13 NMR*. *Macromolecules* **17**, 1479-1489 (1984).
23. K. Schmidt-Rohr, J. Clauss, H. W. Spiess, *Correlation of structure, mobility, and morphological information in heterogeneous polymer materials by two-dimensional wide-line-separation NMR spectroscopy*. *Macromolecules* **25**, 3273-3277 (1992).
24. M. G. Menges, J. Penelle, C. Le Fevere de Ten Hove, A. M. Jonas, K. Schmidt-Rohr, *Characterization of Long-Chain Aliphatic Polyesters: Crystalline and Supramolecular Structure of PE22,4 Elucidated by X-ray Scattering and Nuclear Magnetic Resonance*. *Macromolecules* **40**, 8714-8725 (2007).
25. S. F. Liu, J. D. Mao, K. Schmidt-Rohr, *A Robust Technique for Two-Dimensional Separation of Undistorted Chemical-Shift Anisotropy Powder Patterns in Magic-Angle-Spinning NMR*. *J. Magn. Reson.* **155**, 15-28 (2002).
26. J. D. Mao, K. Schmidt-Rohr, *Separation of aromatic-carbon ^{13}C NMR signals from di-oxygenated alkyl bands by a chemical-shift-anisotropy filter*. *Solid State Nucl. Magn. Reson.* **26**, 36-45 (2004).
27. K. Saalwächter, *Proton multiple-quantum NMR for the study of chain dynamics and structural constraints in polymeric soft materials*. *Prog. Nucl. Magn. Reson. Spectrosc.* **51**, 1-35 (2007).
28. K. Schmidt-Rohr, H. W. Spiess, *Multidimensional Solid-State NMR and Polymers*. (Academic Press, 1994).

- 532 29. E. R. deAzevedo, W. G. Hu, T. J. Bonagamba, K. Schmidt-Rohr, *Centerband-Only Detection of*
533 *Exchange: Efficient Analysis of Dynamics in Solids by NMR*. J. Am. Chem. Soc. **121**, 8411-8412 (1999).
- 534 30. W. S. Veeman, E. M. Menger, W. Ritchey, E. de Boer, *High-Resolution Carbon-13 Nuclear Magnetic*
535 *Resonance of Solid Poly(oxymethylene)*. Macromolecules **12**, 924-927 (1979).
- 536 31. U. Haebleren, *High Resolution Nmr in Solids Selective Averaging*. (Elsevier, 1976).
- 537 32. K. K. Kumashiro *et al.*, *A Novel Tool for Probing Membrane Protein Structure: Solid-State NMR with*
538 *Proton Spin Diffusion and X-Nucleus Detection*. J. Am. Chem. Soc. **120**, 5043-5051 (1998).
- 539 33. Y.-I. Hong, W. Chen, S. Yuan, J. Kang, T. Miyoshi, *Chain Trajectory of Semicrystalline Polymers As*
540 *Revealed by Solid-State NMR Spectroscopy*. ACS Macro Lett. **5**, 355-358 (2016).
- 541 34. D. Reichert, T. J. Bonagamba, K. Schmidt-Rohr, *Slow-down of ¹³C spin diffusion in organic solids by fast*
542 *MAS: a CODEX NMR Study*. J. Magn. Reson. **151**, 129-135 (2001).
- 543 35. D. M. Gezovich, P. H. Geil, *Deformation of polyoxymethylene by rolling*. J. Mater. Sci. **6**, 509-530 (1971).
- 544 36. F. Houry, J. D. Barnes, *The formation of curved polymer crystals: Polyoxymethylene*. J. Res. Nat'l. Stand.
545 Sec. A **78A**, 95-127 (1974).
- 546 37. R. C. Savage, N. Mullin, J. K. Hobbs, *Molecular Conformation at the Crystal–Amorphous Interface in*
547 *Polyethylene*. Macromolecules **48**, 6160-6165 (2015).
- 548 38. X. Zeng, G. Ungar, S. J. Spells, S. M. King, *Real-Time Neutron Scattering Study of Transient Phases in*
549 *Polymer Crystallization*. Macromolecules **38**, 7201-7204 (2005).
- 550 39. P. Duan, K. Schmidt-Rohr, *Composite-pulse and partially dipolar dephased multiCP for improved*
551 *quantitative solid-state ¹³C NMR*. J. Magn. Reson. **285**, 68-78 (2017).
- 552 40. M. Goldman, L. Shen, *Spin-Spin Relaxation in LaF₃*. Physical Review **144**, 321-331 (1966).
- 553 41. N. Egger, K. Schmidt-Rohr, B. Blümich, W. D. Domke, B. Stapp, *Solid state NMR investigation of cationic*
554 *polymerized epoxy resins*. J. Appl. Polym. Sci. **44**, 289-295 (1992).
- 555 42. W. Luo, M. Hong, *Determination of the Oligomeric Number and Intermolecular Distances of Membrane*
556 *Protein Assemblies by Anisotropic ¹H-Driven Spin Diffusion NMR Spectroscopy*. J. Am. Chem. Soc. **128**,
557 7242-7251 (2006).
- 558 43. E. Moreno, R. Cordobilla, T. Calvet, F. J. Lahoz, A. I. Balana, *The C form of n-hexadecanoic acid*. Acta
559 Crystallogr., Sect. C: Cryst. Struct. Commun. **62**, o129-o131 (2006).
- 560
- 561

562
563
564
565
566

Supplementary Material for

• Immobilized ^{13}C -Labeled Polyether Chain Ends Confined to the Crystallite surface Detected by Advanced NMR

567
568

• Immobilized ^{13}COO Chain Ends at Crystallite surface

569

Authors

570 Shichen Yuan¹, Klaus Schmidt-Rohr^{1*}

571 *Corresponding author. Email: srohr@brandeis.edu

572

Affiliations

573 1 Department of Chemistry, Brandeis University, Waltham, MA 02453, USA

574
575

Supplementary Material for this article is available at: [URL]

576 1. Quasi-static ^1H Double Quantum (DQ) Filtering with ^{13}C Detection

577 1.1. Theory and Pulse Sequence

578 1.2. Pulse Sequence for ^{13}C -Detected ^1H Spin Diffusion after Quasi-static DQ Filtering

579 2. Simulations of ^1H and ^{13}C Spin Exchange

580 2.1. Simulation of Spin Exchange Using the Exchange-Matrix Formalism

581 2.2. ^1H Spin Diffusion after $T_{2\text{H}}$ Filtering

582 2.3. CODEX Simulations

583 2.3.1. CODEX Simulations with ^{13}C Spin Exchange in a Model System: 1- ^{13}C -Palmitic Acid

584 2.3.2. CODEX Simulations for Two ^{13}C -Ac₂-POM Crystallite Surfaces

585
586 Table S1. Pulse phases for quasi-static ^1H DQ filtering

587
588 Fig. S1. Small angle X-ray scattering profile of Ac₂-POM

589 Fig. S2. $T_{1\text{C}}$ relaxation of the O-CH₂-O and COO carbons in ^{13}C -Ac₂-POM

590 Fig. S3. Deconvolution of O-CH₂-O peaks in selective and in quantitative ^{13}C spectra

591 Fig. S4. Contour plots of 2D SUPER spectra of PCL and ^{13}C -Ac₂-POM

592 Fig. S5. Quasi-static ^1H DQ filtered CP experiment at a MAS frequency of 4 kHz

593 Fig. S6. ^1H NMR spectra of ^{13}C -Ac₂-POM

594 Fig. S7. Normalized CODEX signal S/S_0 of ^{13}COO end groups in ^{13}C -Ac₂-POM at different
595 spinning frequencies

596 Fig. S8. Analysis of chain end clustering in 1- ^{13}C -palmitic acid and ^{13}C -Ac₂-POM by
597 simulation of CODEX ^{13}C NMR intensity decays

598 Fig. S9. Schematic illustrations of chain ends at the crystallite surface in the POM crystal
599 structure

600 References (34, 42, 43)

601

602